



Inhibition of UV-Induced Stress Signaling and Inflammatory Responses in SKH-1 Mouse Skin by Topical Small-Molecule PD-L1 Blockade

Sally E. Dickinson^{1,2,3}, Prajakta Vaishampayan¹, Jana Jandova^{1,4}, Yuchen (Ella) Ai¹, Viktoria Kirschnerova¹, Tianshun Zhang⁵, Valerie Calvert⁶, Emanuel Petricoin III⁶, H-H. Sherry Chow^{1,7}, Chengcheng Hu^{1,8}, Denise Roe^{1,8}, Ann Bode⁵, Clara Curiel-Lewandrowski^{1,3,9} and Georg T. Wondrak^{1,3,4}

The immune checkpoint ligand PD-L1 has emerged as a molecular target for skin cancer therapy and might also hold promise for preventive intervention targeting solar UV light–induced skin damage. In this study, we have explored the role of PD-L1 in acute keratinocytic photodamage testing the effects of small-molecule pharmacological inhibition. Epidermal PD-L1 upregulation in response to chronic photodamage was established using immunohistochemical and proteomic analyses of a human skin cohort, consistent with earlier observations that PD-L1 is upregulated in cutaneous squamous cell carcinoma. Topical application of the small-molecule PD-L1 inhibitor BMS-202 significantly attenuated UV-induced activator protein-1 transcriptional activity in SKH-1 bioluminescent reporter mouse skin, also confirmed in human HaCaT reporter keratinocytes. RT-qPCR analysis revealed that BMS-202 antagonized UV induction of inflammatory gene expression. Likewise, UV-induced cleavage of procaspase-3, a hallmark of acute skin photodamage, was attenuated by topical BMS-202. NanoString nCounter transcriptomic analysis confirmed downregulation of cutaneous innate immunity- and inflammation-related responses, together with upregulation of immune response pathway gene expression. Further mechanistic analysis confirmed that BMS-202 antagonizes UV-induced PD-L1 expression both at the mRNA and protein levels in SKH-1 epidermis. These data suggest that topical pharmacological PD-L1 antagonism using BMS-202 shows promise for skin protection against photodamage.

Keywords: Inflammation, PD-L1, SKH-1 mouse, Skin photoprotection, UV light

JID Innovations (2024);4:100255 doi:10.1016/j.xjidi.2023.100255

INTRODUCTION

Nonmelanoma skin cancer, primarily comprised of cutaneous squamous cell carcinoma (cSCC) and basal cell

carcinoma, is the most common malignancy worldwide (Madan et al, 2010). Diagnosis and treatment of these keratinocytic neoplasms result in healthcare costs of \$8.1 billion per year in the United States (Guy et al, 2015). Cutaneous exposure to solar UVR is the lead causative factor in skin carcinogenesis, and inflammatory dysregulation is an accepted key mechanism underlying the detrimental effects of acute and chronic UV exposure (Cadet et al, 2012; Clydesdale et al, 2001; Rhodes et al, 2009; Wondrak et al, 2006). We are interested in pursuing molecular methods to prevent and treat cSCCs, which account for 20% of all nonmelanoma skin cancers and kill more than 15,000 people a year (Karia et al, 2013; Mansouri and Housewright, 2017).

PD-L1 (also known as CD274 or B7-H1) is a transmembrane protein involved in the regulation of T-cell responses. Binding of PD-L1 to its receptor, PD-1, on the surface of T cells suppresses T-cell proliferation and activity, an interaction often referred to as an immune checkpoint. The PD-1/PD-L1 interaction as a negative regulator of immune cell activation (and therefore an effector of immune evasion) is now an established target in the cancer therapy field.

Expression of PD-1 is typically restricted to immune cells (including T cells, B cells, and NK cells), and immunotherapies using systemic mAbs against PD-1 have been approved for many advanced malignancies, including cSCC, basal cell carcinoma, and melanoma (Blum et al, 2018; Constantinidou et al, 2019; Vaishampayan et al, 2023). In contrast, PD-L1 is

¹The University of Arizona Cancer Center, The University of Arizona, Tucson, Arizona, USA; ²Department of Pharmacology, College of Medicine Tucson, The University of Arizona, Tucson, Arizona, USA; ³Skin Cancer Institute, University of Arizona, Tucson, Arizona, USA; ⁴Department of Pharmacology & Toxicology, R. Ken Coit College of Pharmacy, The University of Arizona, Tucson, Arizona, USA; ⁵The Hormel Institute, University of Minnesota, Austin, Minnesota, USA; ⁶Center for Applied Proteomics and Molecular Medicine, College of Medicine, George Mason University, Fairfax, Virginia, USA; ⁷Department of Molecular & Cellular Biology, College of Medicine, The University of Arizona, Tucson, Arizona, USA; ⁸Department of Epidemiology and Biostatistics, Mel and Enid Zukerman College of Public Health, The University of Arizona, Tucson, Arizona, USA; and ⁹Division of Dermatology, Department of Medicine, College of Medicine Tucson, The University of Arizona, Tucson, Arizona, USA

Correspondence: Sally E. Dickinson, The University of Arizona Cancer Center, The University of Arizona, 1515 North Campbell Avenue, AZCC Room 4977b, Tucson, Arizona 85724, USA. E-mail: sdickinson@uacc.arizona.edu

Abbreviations: AP-1, activator protein-1; cSCC, cutaneous squamous cell carcinoma; IHC, immunohistochemical; RPPA, reverse-phase protein microarray; SP, sun-protected; SSL, solar-simulated light; TLR, toll-like receptor

Received 25 August 2023; revised 24 November 2023; accepted 5 December 2023; accepted manuscript published online XXX; corrected proof published online XXX

Cite this article as: *JID Innovations* 2024;4:100255

either basally expressed or inducible in most cells of the body. Overexpression of PD-L1 in cSCC is common, and recent literature has shown a correlation between increased PD-L1 expression and advanced clinical risk assessment in these tumors (Dickinson et al, 2021; Schaper et al, 2017; Slater and Googe, 2016; Stravodimou et al, 2021). In addition to PD-1–directed interventions, blockade of PD-L1 by immunotherapeutics is now used clinically in many types of cancer (including melanoma and basal cell carcinoma) and is being studied for use as adjuvant therapy for treatment of cSCC (Lin et al, 2021; Vaishampayan et al, 2023).

In normal skin, PD-L1 expression has been studied extensively in mouse models and only recently in human samples. The PD1/PD-L1 pathway is critical for regulating skin inflammation, and PD-L1 on keratinocytes has been shown to regulate autoimmunity (Imai et al, 2015; Okiyama and Katz, 2014). Transgenic overexpression of PD-L1 in mouse keratinocytes has been shown to reduce acute skin inflammatory responses, yet increase the rates of skin tumorigenesis and risk of death after skin stimulation with a chemical carcinogen (Cao et al, 2011a). Thus, others have suggested that PD-L1 in keratinocytes may allow for resolution of inflammatory signaling upon acute stress in the skin while paving the way for immune evasion of precancerous cells during skin cancer progression (Cao et al, 2011b).

Although little is known about the overall trajectory of PD-L1 expression during the development of cSCC, there is evidence that this ligand may have the potential as a target for skin cancer prevention strategies (Cao et al, 2011b; Malaspina et al, 2011; Ritprajak and Azuma, 2015). Recent evidence indicates that exposure to acute UV through solar-simulated light (SSL) in human and mouse skin causes significant upregulation of PD-L1 protein in epidermal keratinocytes from its low baseline expression levels. This suggests that a primary environmental causative factor driving skin carcinogenesis, UV light, is sufficient to modulate PD-L1 in the epidermis (Dickinson et al, 2021). In this study, we present evidence that PD-L1 expression is increased in chronically sun-damaged, noncancerous human skin, thus supporting the role of PD-L1 as a potential target for immunoregulation and skin cancer prevention. Although clinically relevant mAbs to PD-L1 are effective for systemic treatment of existing tumors, antibodies are not ideal for preventive strategies or for topical application to at-risk areas. We therefore tested whether topical application of a PD-L1–specific small-molecule pharmacological inhibitor, BMS-202, can affect UV-induced stress responses *in vitro* and in mouse skin. Our findings provide evidence that topical BMS-202 provides protection against UV-induced inflammatory stress responses in acutely treated skin, an effect that is also associated with downregulation of UV-induced keratinocytic PD-L1 expression.

RESULTS

PD-L1 expression is significantly increased in human cSCC as well as sun-damaged epidermis compared with that in sun-protected skin

First, differential PD-L1 expression in human skin comparing normal skin with cSCC was examined by immunohistochemical (IHC) analysis using an in-house library of banked

clinically annotated specimens. Immunohistochemistry of PD-L1 in normal sun-protected (SP) skin was compared with that from samples of low-risk or high-risk cSCCs. Determination of cSCC risk status was defined by pathological microanatomical assessment of each tumor specimen. Epidermal or tumor percentage staining was scored by a board-certified dermatopathologist (Figure 1a and b). Although normal human epidermis shows no PD-L1 expression, low-risk and high-risk cSCCs significantly upregulate this immune checkpoint protein, an observation consistent with earlier reports ($P < .001$) (Dickinson et al, 2021).

To test whether PD-L1 upregulation by UV exposure occurs early in the progression from normal skin to cSCC, we also examined human biopsies of chronically sun-damaged skin. Immunohistochemistry of clinically assessed sun-damaged skin samples revealed a mild upregulation of PD-L1 detectable in basal keratinocytes of the epidermis (Figure 1c). Further analysis of epidermal lysates from a second set of skin samples was performed using reverse-phase protein array (RPPA) to more quantitatively measure PD-L1 protein expression changes. PD-L1 analysis included biopsies from clinically assessed SP, mild sun-damaged, moderate sun-damaged, or severe sun-damaged skin. A waterfall plot depiction of these results illustrates the clustering of the majority of SP samples characterized mostly by low PD-L1 expression, whereas the sun-damaged samples exhibited higher PD-L1 expression (Figure 1d, left). Box and whisker plot depiction indicates that sun-damaged epidermis expresses significantly more PD-L1 than SP epidermis (Figure 1d, right) ($P \leq .0001$), whereas PD-L1 expression between sun-damaged subgroups did not differ significantly. Furthermore, analysis of additional samples derived from the same donor set, exposed to acute SSL (2 MED) and then RPPA probed for PD-L1 expression, revealed statistically significant PD-L1 upregulation in response to UV that occurred irrespective of SP or sun-damaged status (data not shown).

The PD-L1 antagonist BMS-202 blocks UV-induced AP-1–responsive stress signaling, expression of inflammatory mediators, and apoptosis in mouse skin

A recent report has indicated that acute SSL exposure causes strong stimulation of epidermal PD-L1 expression in mouse and human skin as assessed by immunohistochemistry (Dickinson et al, 2021). Because the sun-damaged skin mentioned earlier indicates that PD-L1 upregulation may occur early in the etiology of skin cancer progression, we were interested in assessing whether topical pharmacological inhibitors of PD-L1 could affect UV responses in the skin. Among numerous small-molecule PD-L1 antagonists available commercially, after screening on the basis of physicochemical properties (absence of UVA/UVB absorbance [data not shown], favorable logP [3.6], minimal systemic availability upon topical application, lack of cellular toxicity, and prior systemic use in animal models), we selected BMS-202 as a potent nonpeptidic inhibitor to examine how blocking the activity of PD-L1 would affect skin UV responses (Figure 2a) (all pharmacokinetic data to be published elsewhere) (Ashizawa et al, 2019; Guzik et al, 2017; Zak et al, 2017).

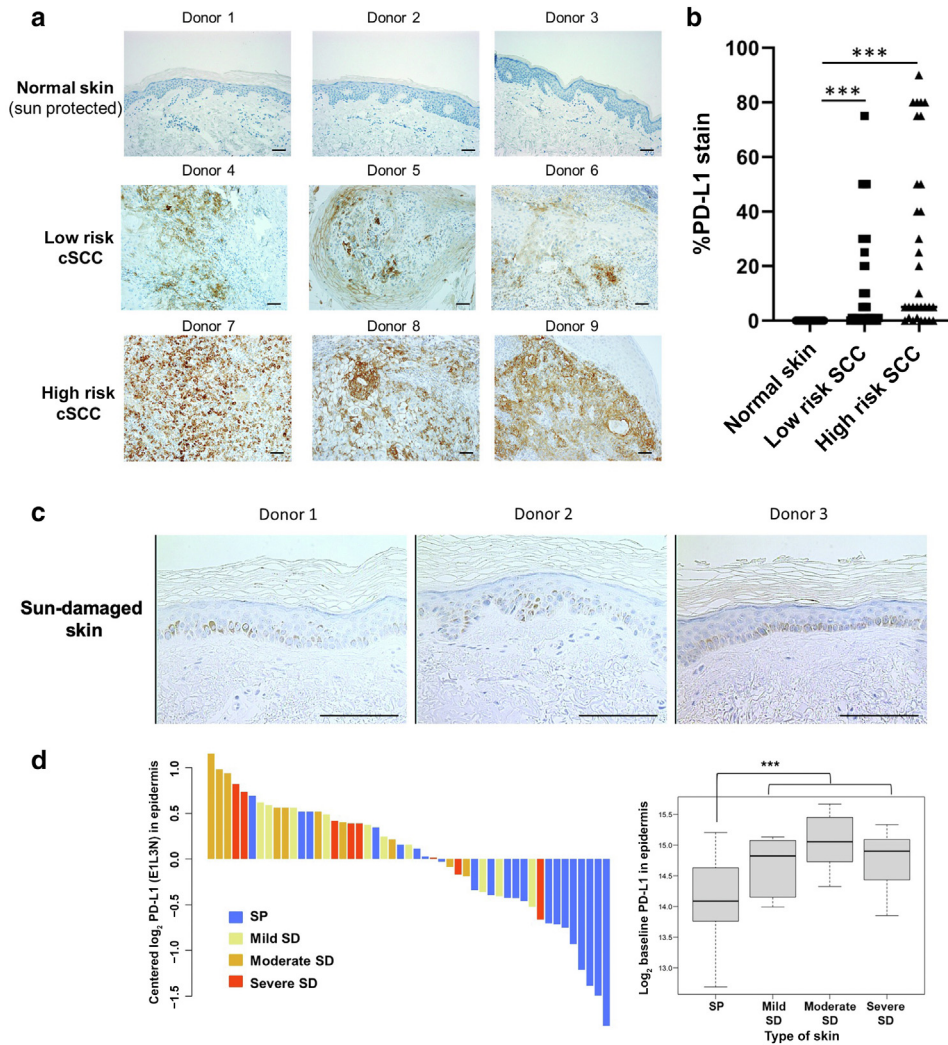


Figure 1. PD-L1 expression in human skin increases as a function of cSCC progression and is detectable in SD versus SP skin. (a) PD-L1 expression from a clinical cohort stratified as normal skin, low-risk cSCC, or high-risk cSCC (IHC; 9 representative donor specimens, bar = 100 μ m, analysis performed as previously published [Dickinson et al, 2021]). (b)

Quantitative analysis of tissue staining (panel A), normal skin: n = 20, low-risk SCC: n = 40, and high-risk SCC: n = 31 (** P < .001, Kruskal–Wallis nonparametric data analysis). (c) PD-L1 expression in SD skin (IHC; bar = 100 μ m, 3 representative donors). (d) Proteomic (RPPA) analysis of PD-L1 expression in human epidermal samples stratified by SD status (SP or SD). Left: waterfall plot depicting epidermal PD-L1 expression per human skin biopsy; right: box-and-whisker depiction indicating median (line in box) with interquartile range as well as maximum and minimum values (** P < .001). See Materials and Methods for clinical details. cSCC, cutaneous squamous cell carcinoma; IHC, immunohistochemistry; RPPA, reverse-phase protein array; SCC, squamous cell carcinoma; SD, sun damaged; SP, sun protected.

The activator protein-1 (AP-1) transcription factor plays a part in normal cellular metabolism but is also stimulated in response to cellular stressors, including environmental UV exposure (Cooper and Bowden, 2007; Dickinson et al, 2009; Shaulian and Karin, 2001; Snell et al, 2023; Zhong et al, 2001). Notably, PD-L1 is regulated by several transcription factors and signaling pathways known to be stimulated by UV, including AP-1 (Green et al, 2012; Ritprajak and Azuma, 2015). We maintain transgenic mice that harbor a ubiquitously expressed luciferase reporter gene under the control of the AP-1 transcription factor-driven TPA-Response Element. This transgene has been bred onto the outbred SKH-1 hairless immunocompetent mouse line and displays a luciferin-dependent bioluminescent response when exposed to UV light. This model is a valuable tool for testing topical agents in vivo for their stimulatory or inhibitory effects on stress responses in the skin (Jandova et al, 2021; Snell et al, 2023). We therefore treated these AP-1 reporter mice topically with either vehicle or BMS-202, with or without subsequent UVB exposure. Mice were imaged for bioluminescence using luciferin injection 24 hours later. Notably, BMS-202 significantly inhibited the UV-induced AP-1-related inflammatory stress response, causing an almost 5-fold attenuation in

bioluminescent signal intensity (Figure 2b). We also confirmed this response in vitro using HaCaT human keratinocytes stably transfected with the AP-1-responsive luciferase construct (Chen et al, 1998), which also showed significant inhibition of UVB-induced signal intensity as a consequence of BMS-202 treatment (Figure 2c).

After the AP-1 luciferase assays mentioned earlier, we also probed the expression of select inflammatory and immune-related genes by independent RT-qPCR analysis of SKH-1 mouse skin, which had been treated with vehicle + SSL or 8 mM BMS-202 + SSL and harvested 24 hours later. These analyses included cytokines (*Il1 β* , *Il6*, *Il10*, *Tnfa*) and other inflammatory mediators (*Ptgs2*, *Tlr4*), all of which displayed strong downregulation of UV-induced expression as a result of BMS-202 treatment (Figure 2d).

Next, we probed for SSL-induced induction of epidermal cell death by IHC staining for cleaved caspase-3, an established marker of UV-induced apoptotic cell death observable in SKH-1 mouse skin (Dickinson et al, 2011; Janda et al, 2016). As expected, staining intensity was negligible in control samples, whereas exposure to vehicle + SSL displayed dramatic stimulation of cleaved caspase-3 at 24 hours. Remarkably, treatment with BMS-202 led to a

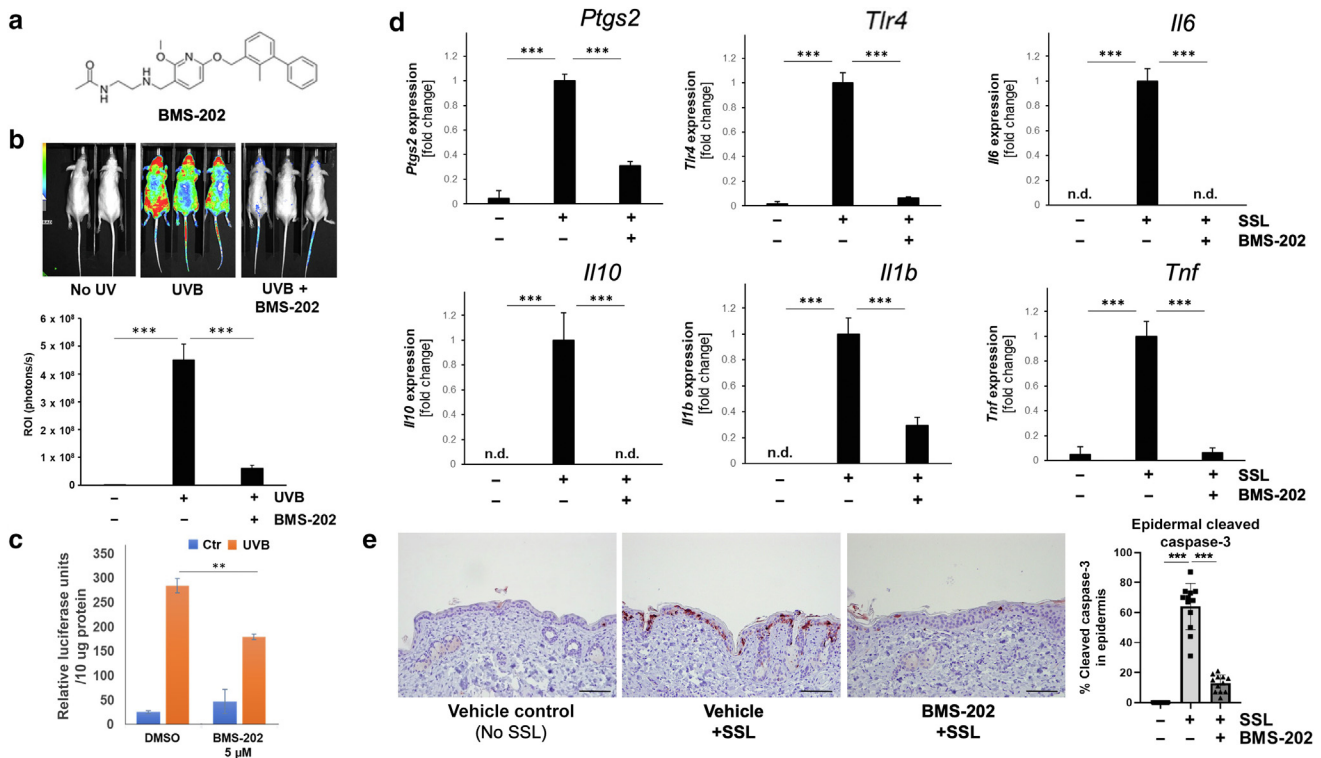


Figure 2. Topical application of the PD-L1 inhibitor BMS-202 antagonizes SSL-induced stress signaling, inflammatory gene expression, and caspase-3 cleavage in SKH-1 mouse skin. (a) BMS-202 molecular structure. (b) Bioluminescent AP-1 reporter mice display SSL-induced inflammatory signaling suppressed by topical BMS-202 (8 mM). Top: representative transgenic AP-1 luciferase SKH-1 reporter mice. Bottom: quantification of bioluminescence intensity. All groups (n = 3) were treated with vehicle (acetone) or vehicle + BMS-202. (c) BMS-202 suppression of inflammatory signaling in AP-1 luciferase reporter HaCaT cells (representative of 3 independent experiments; 3 experimental replicates per group). (d) Gene-specific gene expression analysis by RT-qPCR indicates BMS-202 suppression of SSL-induced genes in SKH-1 mouse skin (n = 3 mice per group). (e) BMS-202 suppression of SSL-induced caspase-3 cleavage—representative skin images (left, bar = 100 μm) and quantification (right, n = 3 mice per group). Bar graphs depict mean ± SD (**P ≤ .001 and ***P ≤ .0001). AP-1, activator protein-1; SSL, solar-simulated light.

significant reduction in epidermal positivity for this apoptotic marker, reducing the percentage of epidermal cells staining positive for cleaved caspase-3 from over 60% to approximately 10% (Figure 2e).

Topical BMS-202 treatment suppresses UV-associated gene expression changes in SKH-1 mouse skin as identified by NanoString transcriptomic analysis

Next, to more broadly assess the consequences of topical BMS-202 treatment on gene expression in UV-exposed SKH-1 mouse skin, NanoString nCounter analysis using the nCounter Mouse Inflammation V2 panel (probing 254 genes for focused screening of the inflammation and immune response, including 6 internal reference controls) was performed. To this end, SKH-1 mice were treated topically with 8 mM BMS-202 or carrier and exposed to SSL as described in the Materials and Methods, and comparative NanoString expression analysis was performed 24 hours after irradiation. Overall expression analysis employing heatmap (z-score) and volcano plot depictions show significant changes between the treatment groups (Figure 3).

Clustered analysis of statistically significant expression changes indicated that 75 genes displayed BMS-202 responsiveness in SKH-1 mouse skin (≥4-fold differential vs vehicle control [upregulated: 23; downregulated: 52]) (tabular summary is presented in Tables 1 and 2). Using

nCounter Advanced Analysis software, overall (Figure 4a and b) and single pathway score profiling identified specific UV-responsive gene expression networks differentially modulated as a function of BMS-202 treatment (Figure 4c). Remarkably, major pathways known to be activated in the skin upon exposure to solar UV were downregulated in response to BMS-202, including activation of NF-κB, innate immune response, chemokine activity, inflammatory response, and angiogenesis. In contrast, immune response, known to be antagonized by solar UV exposure, was upregulated in UV-exposed skin as a consequence of BMS-202 treatment (Figure 4c). Expression heatmaps including gene identity assigned to the inflammatory response and immune response by nCounter pathway analysis are depicted in Figures 5 and 6, respectively.

Consistent with these pathway score analyses, downregulated expression in response to BMS-202 treatment impacted genes (fold downregulation) in the following domains, among others: signal transducer and activator of transcription signaling (signal transducer and activator of transcription 1 gene *Stat1* [2.8], signal transducer and activator of transcription 2 gene *Stat2* [2.5], signal transducer and activator of transcription 3 gene *Stat3* [7.4]), AP-1 signaling (*Fos* [4.1], *Jun* [5.9]), other transcription factors (*Myc* [3.3], *Nf2e2* [3.5], *Hif1a* [9.6], *Nfatc3* [4.1]), MAPK signaling (*Raf1* [5.7], *Rac1* [7.3], *Gnas* [11.5], *Gnb1* [5.8], *Mapk8*

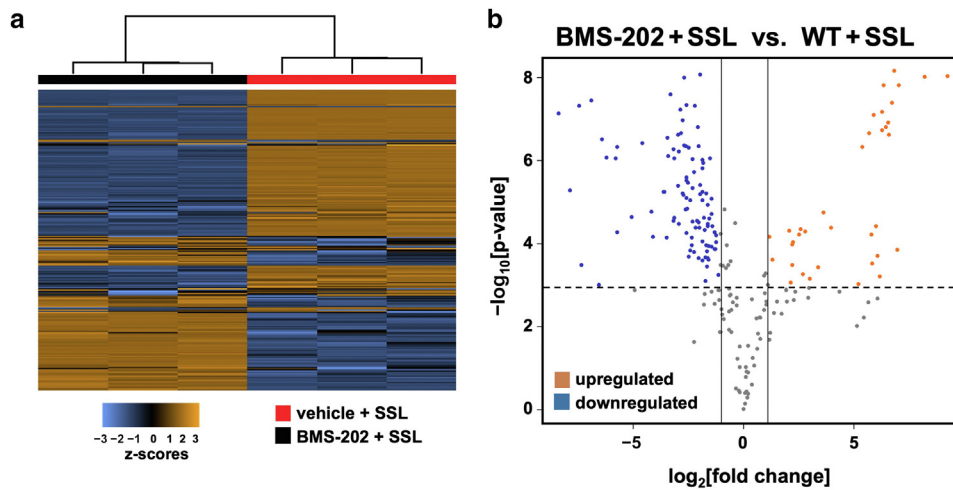


Figure 3. NanoString nCounter expression analysis of SKH-1 mouse skin after SSL exposure with or without topical BMS-202 treatment. (a) Overall heatmap with z-score. (b) Volcano plot depiction. Analysis was performed using 3 independent murine specimens per group. SSL, solar-simulated light.

[3.1], *Mapk1* [3.7], *Map3k7* [3.7], *Map3k1* [4.5], *Mapkapk2* [5.1], *Map2k1* [5.8], *Mapk14* [5.9], *Mapk3* [6.3], *Map3k5* [6.4], *Map2k4* [6.4]), inflammation and tissue remodeling (*Nfkb1* [5.9], matrix metalloproteinase 9 gene *Mmp9* [8.2], matrix metalloproteinase 3 gene *Mmp3* [3.8], *Ptgs1* [3.1], *Ptgs2* [1.7], *Tgfb1* [13.3], *Tgfb3* [2.7], *Pdgfa* [5.2]), innate immune signaling (*Tlr2* [2.4], *Tlr8* [3.4], *Myd88* [2.7], *Ly96* [coreceptor of *Tlr4*; 11.0]), and chemokine and cytokine signaling (*Il1b* [2.9], *Il1r1* [5.5], *Il1rap* [3.6], *Il6ra* [3.4], *Il10rb* [3.2], *Il18* [20.0], *Cxcl1* [4.1], *Cxcl5* [11.6], *Ccl7* [8.1], *Ccl2* [5.3], *Ccl3*, *Ccl8* [5.0], *Il6ra* [3.4]) (Table 1).

Genes displaying upregulated expression by at least 4-fold in response to BMS-202 exposure compared with those for vehicle + SSL included IFN-related immune mediators (*Ifna* [89.3], *Ifnb1* [16.4], *Ifng* [10.6], *Ifi44* [5.2]), ILs (*Il21* [50.1], *Il9* [28.9], *Il23a* [6.5]), chemokines (*Ccr3* [20.5], *Cxcl10* [4.3]), and other immune factors (*Defars1* [51.0], *C8b* [26.2], *C9* [18.6], *Mbl2* [15.7], *Tlr9* [8.3], *Nos2* [6.1], *Tnfsf14* [4.8]) (Table 2).

BMS-202 suppresses UV-induced PD-L1 expression in cultured human keratinocytes and mouse epidermis

Given the pronounced UV responsiveness of epidermal PD-L1 expression detected in previous studies using mouse and human skin (Dickinson et al, 2021) and the remarkable inhibitory effects of BMS-202 on UV-induced stress responses, we next tested the effects of BMS-202 on UV-induced cutaneous PD-L1 expression.

Remarkably, treatment with BMS-202 blocked SSL-induced PD-L1 expression in HaCaT keratinocytes at the mRNA and protein level (Figure 7a and b), an observation that was reproducible in human primary keratinocytes in culture (HEKa cells (Figure 7c). Immunoblot analysis using SKH-1 mouse epidermis confirms that PD-L1 protein, found at low levels in untreated skin, becomes strongly induced 24 hours after SSL exposure (Figure 7d). Strikingly, topical BMS-202 significantly antagonized UV-induced PD-L1 upregulation at the protein level in the SKH-1 mouse epidermis (Figure 7e). This antagonistic effect is more pronounced if the compound is applied before and after UV. Importantly, IHC staining for PD-L1 confirms epidermal stimulation of this protein by acute SSL and its pronounced inhibition by BMS-

202 topical application (24 hours after SSL harvest) (Figure 7f). This inhibition also occurs at the transcriptional level as assessed in full-thickness mouse skin by RT-qPCR (Figure 7g).

DISCUSSION

Immunotherapeutics have played a critical role in advancing the treatment of many malignancies, including high-risk skin cancers. The PD-1/PD-L1 immune checkpoint has been investigated in much detail, and recent literature has shown that cSCC is among the many tumor types to overexpress PD-L1 (Dickinson et al, 2021; Vaishampayan et al, 2023; Zerdas et al, 2018). In contrast, given the keratinocytic origin of cSCC, the responsiveness of epidermal PD-1/PD-L1 expression to carcinogenic environmental stressors (including solar UV light) remains poorly explored, and the effects of PD-1/PD-L1 modulation on skin photodamage are equally unknown. Given that antibody-based modulation of the PD-1/PD-L1 immune checkpoint is now firmly established for therapeutic interventions targeting malignancies, there is an unexplored opportunity for molecular approaches aiming at skin photoprotection and immunoprevention of skin cancer (Umar, 2014).

Therefore, we first examined PD-L1 expression in human epidermis both as a function of chronic sun exposure (SP vs sun damaged) and tumorigenesis (cSCC). Consistent with earlier published observations, these data indicate that PD-L1 is upregulated in cSCC (Figure 1a and b) (Dickinson et al, 2021). Using a proteomic approach (RPPA) allowing for high-sensitivity quantification of human tissue analytes, we then observed that PD-L1 expression is upregulated significantly in sun-damaged skin compared with that in SP skin, an observation indicative of chronic UV-induced PD-L1 induction before epidermal tumorigenesis (Figure 1c and d).

On the basis of the observation that PD-L1 expression displays UV responsiveness in human skin, we undertook an examination of the effects of PD-L1 antagonism on acute consequences of cutaneous solar UV exposure. To this end, we selected BMS-202, a small-molecule PD-L1 antagonist amenable for topical use in SKH-1 mouse skin (Figure 2a). Strikingly, UV-induced reporter gene expression controlled

Table 1. Genes Downregulated in BMS-202 + SSL Skin Relative to Those in SSL Control (NanoString Analysis)

Gene	Gene ID	Gene Name	Fold Change	P-Value
<i>Irf1</i>	16362	IFN regulatory factor 1	-4.1	1.47E-06
<i>Nfatc3</i>	18021	Nuclear factor of activated T cells, calcineurin dependent 3	-4.1	2.50E-05
<i>Cxcl1</i>	14825	Chemokine (C-X-C motif) ligand 1	-4.1	6.68E-06
<i>Fos</i>	14281	FBJ osteosarcoma oncogene	-4.1	1.95E-05
<i>Oas1a</i>	246730	2'-5' oligoadenylate synthetase 1A	-4.3	1.71E-05
<i>Tcf4</i>	21413	Transcription factor 4	-4.4	7.84E-06
<i>Trem2</i>	83433	Triggering receptor expressed on myeloid cells 2	-4.5	7.51E-07
<i>C1qa</i>	12259	Complement component 1, q subcomponent, alpha	-4.5	2.91E-06
<i>Grb2</i>	14784	GF receptor bound protein 2	-4.5	1.30E-04
<i>Map3k1</i>	26401	Mitogen-activated protein kinase 1	-4.5	2.21E-04
<i>Cdc42</i>	12540	Cell division cycle 42	-4.6	7.29E-09
<i>Tyropb</i>	22177	TYRO protein tyrosine kinase binding protein	-4.9	7.68E-08
<i>Nr3c1</i>	14815	Nuclear receptor subfamily 3, group C, member 1	-4.9	1.08E-05
<i>Ccl8</i>	20307	Chemokine (C-C motif) ligand 8	-5.0	8.38E-06
<i>Nod2</i>	257632	Nucleotide-binding oligomerization domain containing 2	-5.1	1.15E-04
<i>Pdgfa</i>	18590	Platelet-derived growth factor, alpha	-5.2	2.52E-07
<i>Mapkapk2</i>	17164	MAP kinase-activated protein kinase 2	-5.2	2.01E-06
<i>Ccl2</i>	20296	Chemokine (C-C motif) ligand 2	-5.3	1.22E-07
<i>Mrc1</i>	17533	Mannose receptor, C type 1	-5.4	2.24E-06
<i>Il1r1</i>	16177	IL-1 receptor, type I	-5.5	5.11E-06
<i>Raf1</i>	110157	v-Raf-leukemia viral oncogene 1	-5.7	7.03E-06
<i>Gnb1</i>	14688	Guanine nucleotide binding protein (G protein), beta 1	-5.8	1.42E-07
<i>Map2k1</i>	26395	Mitogen-activated protein kinase 1	-5.8	5.49E-08
<i>Mapk14</i>	26416	Mitogen-activated protein kinase 14	-5.9	2.33E-06
<i>Nfkb1</i>	18033	NF-kappaB1, p50/p105	-5.9	2.59E-06
<i>Rhoa</i>	11848	Ras homolog family member A	-5.9	5.95E-07
<i>Jun</i>	16476	Jun proto-oncogene	-5.9	1.97E-06
<i>C4a</i>	625018	Complement component 4A	-5.9	4.41E-07
<i>Mapk3</i>	26417	Mitogen-activated protein kinase 3	-6.3	2.30E-07
<i>Map3k5</i>	26408	Mitogen-activated protein kinase 5	-6.4	2.86E-05
<i>Map2k4</i>	26398	Mitogen-activated protein kinase 4	-6.4	3.72E-08
<i>Rac1</i>	19353	Rac family small GTPase 1	-7.3	1.92E-08
<i>Shc1</i>	20416	src homology 2 domain-containing transforming protein C1	-7.4	1.09E-05
<i>Stat3</i>	20848	Signal transducer and activator of transcription 3	-7.4	6.97E-09
<i>Ccl7</i>	20306	Chemokine (C-C motif) ligand 7	-8.1	2.23E-04
<i>Itgb2</i>	16414	Integrin beta 2	-8.2	1.52E-06
<i>Mmp9</i>	17395	Matrix metalloproteinase 9	-8.2	4.35E-06
<i>Cebpb</i>	12608	CCAAT/enhancer binding protein (C/EBP), beta	-8.3	2.18E-06
<i>C3</i>	12266	Complement component 3	-9.0	2.68E-07
<i>Cxcl3</i>	330122	Chemokine (C-X-C motif) ligand 3	-9.1	2.48E-05
<i>Hif1a</i>	15251	Hypoxia-inducible factor 1, alpha subunit	-9.6	2.24E-08
<i>Cfl1</i>	12631	Cofilin 1, non-muscle	-10.8	3.04E-09
<i>Ly96</i>	17087	Lymphocyte antigen 96	-11.0	3.59E-05
<i>Gnas</i>	14683	Guanine nucleotide binding protein, alpha stimulating	-11.5	1.31E-06
<i>Cxcl5</i>	20311	Chemokine (C-X-C motif) ligand 5	-11.6	1.65E-07
<i>Ppp1r12b</i>	329251	Protein phosphatase 1, regulatory subunit 12B	-12.1	1.54E-05
<i>Bcl6</i>	12053	B-cell leukemia/lymphoma 6	-12.8	2.85E-05
<i>Tgfb1</i>	21803	Transforming GF, beta 1	-13.3	2.02E-05
<i>H2-Eb1</i>	14969	Histocompatibility 2, class II antigen E beta	-14.2	5.42E-08
<i>Fxyd2</i>	11936	FXD domain-containing ion transport regulator 2	-17.0	3.07E-05
<i>Il18</i>	16173	IL-18	-20.0	6.86E-06
<i>Mef2c</i>	17260	Myocyte enhancer factor 2C	-64.9	7.36E-05

Abbreviations: ID, identification; SSL, solar-simulated light.

Fold changes with adjusted *P*-values are reported.

by AP-1 transcriptional activity was strongly suppressed by topical BMS-202 in vivo (Figure 2b), a result also confirmed in vitro (Figure 2c). Consistent with BMS-202 suppression of

keratinocytic inflammatory UV responses, gene-specific RT-qPCR-based expression analysis indicated attenuated expression of genes, including *Il6*, *Il10*, *Il1b*, *Tnf*, *Ptgs2*

Table 2. Genes Upregulated in BMS-202 + SSL Skin Relative to Those in SSL Control (NanoString Analysis)

Gene	Gene ID	Gene Name	Fold Change	P-Value
<i>Ifna1</i>	15962	IFN alpha 1	89.3	1.58E-05
<i>Defa-rs1</i>	13218	Defensin, alpha, 29	51.0	9.12E-06
<i>Il21</i>	60505	IL21	50.1	7.69E-06
<i>Mx1</i>	17857	MX dynamin-like GTPase 1	36.2	3.37E-06
<i>Il9</i>	16198	IL9	28.9	3.24E-05
<i>C8b</i>	110382	Complement component 8, beta polypeptide	26.2	3.64E-05
<i>Crp</i>	12944	C-reactive protein, pentraxin-related	23.9	3.08E-06
<i>Ccr3</i>	12771	Chemokine (C-C motif) receptor 3	20.5	2.98E-05
<i>C9</i>	12279	Complement component 9	18.6	1.81E-05
<i>Ifnb1</i>	15977	IFN beta 1, fibroblast	16.4	3.73E-06
<i>Mbl2</i>	17195	Mannose-binding lectin (protein C) 2	15.7	5.08E-05
<i>Kng1</i>	16644	Kininogen 1	14.9	1.58E-05
<i>Cysltr2</i>	70086	Cysteinyl leukotriene receptor 2	14.4	1.66E-04
<i>Ifng</i>	15978	IFN gamma	10.6	5.95E-05
<i>Chi3l3</i>	12655	Chitinase-like 3	10.5	4.86E-07
<i>Tlr9</i>	81897	Toll-like receptor 9	8.3	2.54E-04
<i>Il23a</i>	83430	IL 23, alpha subunit p19	6.5	3.23E-04
<i>Nos2</i>	18126	Nitric oxide synthase 2, inducible	6.1	8.12E-04
<i>Mx2</i>	17858	MX dynamin-like GTPase 2	5.3	3.00E-04
<i>Ifi44</i>	99899	IFN-induced protein 44	5.2	3.77E-03
<i>Tnfsf14</i>	50930	TNF superfamily, member 14	4.8	3.15E-03
<i>Cxcl10</i>	15945	Chemokine (C-X-C motif) ligand 10	4.3	4.06E-04
<i>Tslp</i>	53603	Thymic stromal lymphopoietin	4.3	2.15E-06

Abbreviations: ID, identification; mmp9, matrix metalloproteinase 9; SSL, solar-simulated light. Fold changes with adjusted *P*-values are reported.

(encoding cyclooxygenase-2), and *Tlr4* (Figure 2d). In addition, another hallmark of acute skin photodamage, that is, UV-induced keratinocytic apoptosis, was suppressed by topical BMS-202, as evidenced by reduced epidermal levels of cleaved caspase-3 compared with that in vehicle-treated UV-exposed mice (Figure 2e).

A more extensive NanoString-based inflammation-focused transcriptomic follow-up analysis employing nCounter gene expression pathway identification (Mouse Inflammation V2 panel) indicated that topical BMS-202 application caused a pronounced modulation of UV-induced mRNA changes in SKH-1 skin. These expression changes were characterized by suppression of innate and inflammatory responses, NF- κ B activation, chemokine activity, and angiogenesis (Figures 3–6 and Tables 1 and 2). In contrast, immune response pathway gene expression was upregulated (including *Ifna1*, *Ifnb1*, and *Ifng*, among others), consistent with BMS-202 antagonism of PD-L1 blockade of adaptive immune responses mediated mostly by lymphocytes (Figure 4). Thus, because UV exposure is known to be associated with acute suppression of adaptive immune function, these data could be indicative of BMS-202 preserving skin immunity after acute photodamage while suppressing keratinocytic inflammatory responses (AP-1 activation, *Ptgs2* expression, etc) (Figure 2). Further studies examining PD-L1 expression in acutely photodamaged mouse skin revealed that acute UV exposure upregulates PD-L1 expression at both the mRNA and protein levels in the epidermis, an observation confirmed by keratinocytes in culture. Strikingly, this effect was antagonized by BMS-202, with topical application

blocking UV-induced PD-L1 upregulation, an observation also replicated in cell culture (Figure 7).

The role of PD-L1—related responses to photodamage in the skin (acute vs chronic responses) remains to be explored. Given its role as an established checkpoint ligand and its function in the control of cutaneous adaptive immune responses that involve numerous cells (eg, antigen-presenting cells, lymphocytes, mast cells, etc), it is expected that UV-induced PD-L1 stimulation has a significant impact on skin inflammatory stress responses. In our study, we observed that PD-L1 antagonism using BMS-202 causes suppression of UV-induced inflammation on the basis of AP-1 reporter assays and transcriptomic analysis. However, the role of keratinocytic PD-L1 impacting chronic photodamage responses remains to be addressed by future experiments.

BMS-202 is a small-molecule inhibitor that has been shown to bind the hydrophobic pocket of PD-L1, causing aberrant homodimerization and preventing the ability of PD-L1 to interact with the PD-1 receptor (see structure [Figure 2a]). BMS-202 is a potent and nonpeptidic inhibitor with a half-maximal inhibitory concentration of 18 nM and a K_D of 8 μ M. This biphenyl compound binds to the region that typically interacts with PD-1 (Guzik et al, 2017; Zak et al, 2017) and promotes antitumor activity in mouse models but has not been used either topically or for preventive purposes (Ashizawa et al, 2019). BMS-202 has been used previously for systemic interventions in orthotopic xenograft models and has shown effective tumoral inhibition in several models if employed as a single or combination agent (Hu et al, 2020; Padmanabhan et al, 2022; Sun et al, 2023;

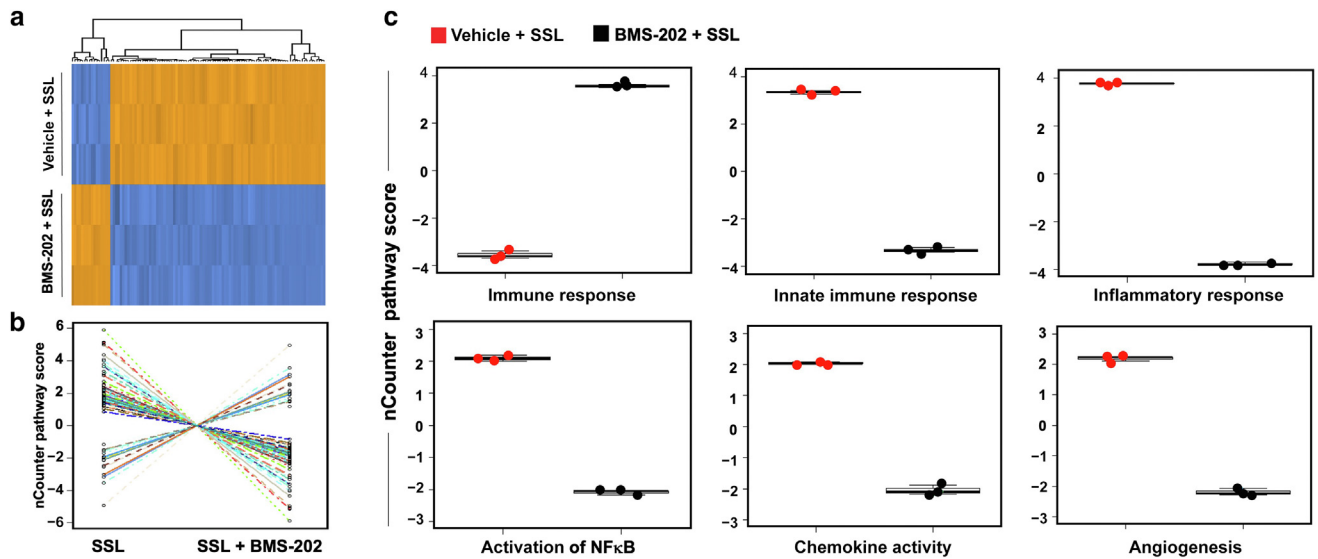


Figure 4. NanoString nCounter expression analysis of SKH-1 mouse skin after SSL exposure with or without topical BMS-202 treatment. (a) Heatmap of pathway scores: clustered analysis of statistically significant expression changes as a function of BMS-202 exposure (8 mM; blue: low scores, orange: high scores); scores are displayed on the same scale through a Z-transformation. (b) Overall pathway score analysis: covariate plot. (c) Single pathway score analysis ($P < .05$). Analysis was performed using 3 independent murine specimens per group. SSL, solar-simulated light.

Zhang et al, 2019). Remarkably, even though BMS-202 has been shown to disrupt PD-L1 interaction with PD-1 (thereby blocking immune checkpoint activity), we also observed that it reduces UV-induced *Pdl1* mRNA and protein levels, but the molecular mechanism underlying this effect remains to be established. It has now been observed that BMS-

202—inspired structural analogs can induce PD-L1 internalization followed by protein degradation that might also impact mRNA levels, a mechanism of action to be substantiated in epidermal keratinocytes exposed to UV and BMS-202 (Dai et al, 2022; Gou et al, 2020; Hanks, 2022; Hudson et al, 2020; Sun et al, 2023). Whether BMS-202 acts

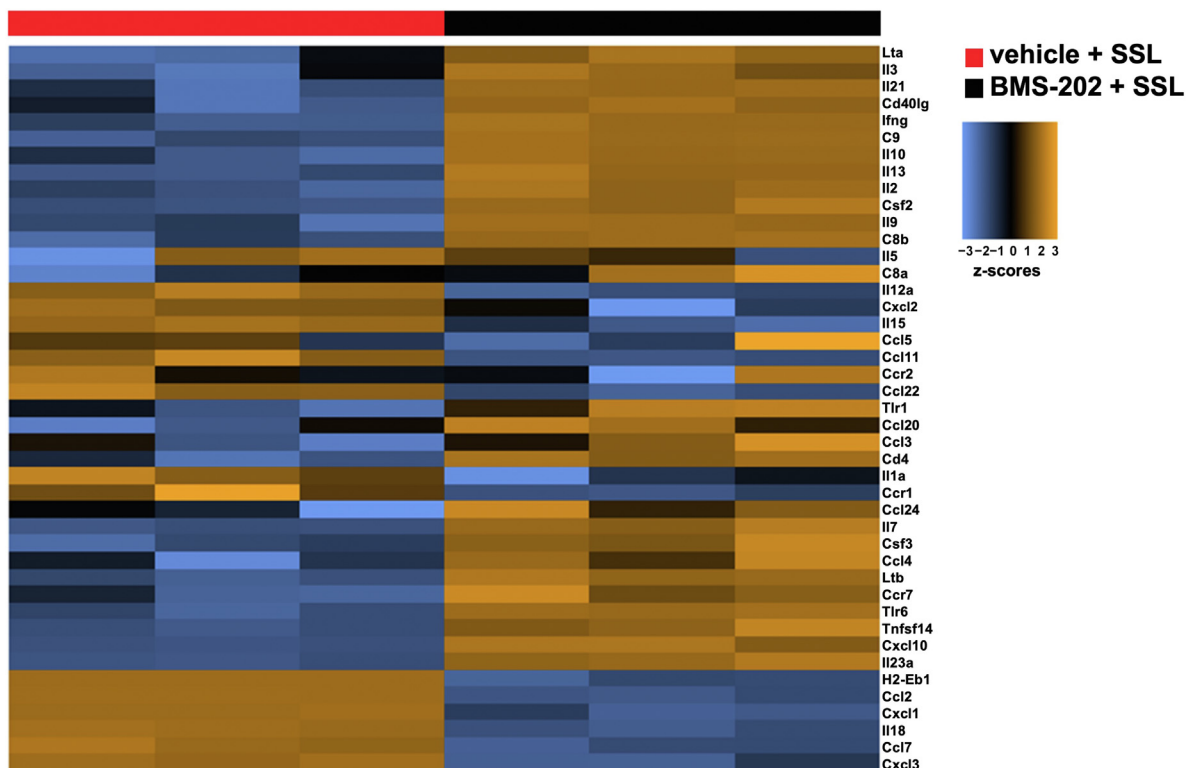


Figure 5. Heatmap depiction of immune response pathway expression data. Heatmap of the normalized data with z-score (vehicle + SSL vs BMS-202 + SSL), scaled to give all genes equal variance, generated through unsupervised clustering. Orange indicates high expression; blue indicates low expression. Analysis was performed using 3 independent murine specimens per group. SSL, solar-simulated light.

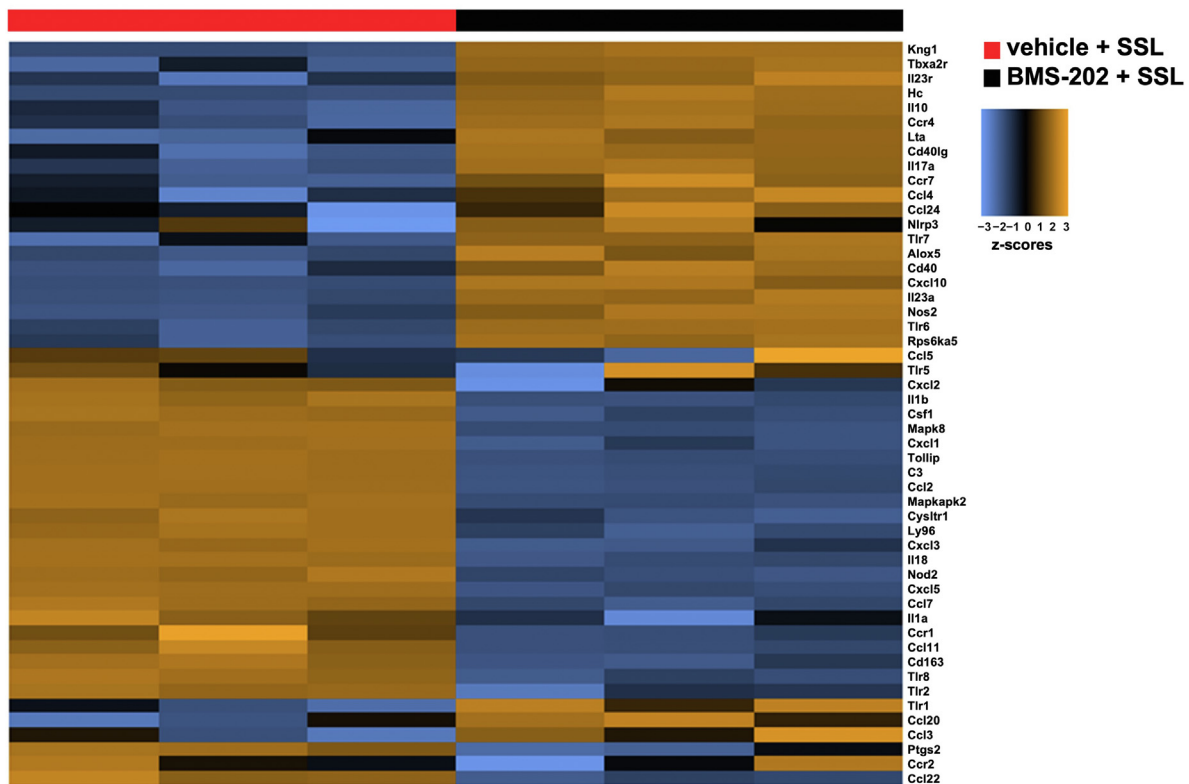


Figure 6. Heatmap depiction of inflammatory response pathway expression data. Heatmap of the normalized data with z-score (vehicle + SSL vs BMS-202 + SSL), scaled to give all genes equal variance, generated through unsupervised clustering. Orange indicates high expression; blue indicates low expression. Analysis was performed using 3 independent murine specimens per group. SSL, solar-simulated light.

through this additional blockade of intrinsic PD-L1 activity contributing to its anti-inflammatory and photoprotective activity remains to be explored.

An anticipated advantage of a topical pharmacological approach as pursued in this study is the ability to achieve PD-L1 antagonism confined to focused application to the epidermis only, reducing the risk of systemic exposure and potential off-target effects observable in human patients during therapeutic use of PD-1/PD-L1-directed mAbs. It remains to be seen whether genetic antagonism exclusively targeting epidermal PD-L1 is able to mimic the photoprotective effects achieved in this study by pharmacological PD-L1 inhibition. If applicable to human skin, further studies should substantiate the feasibility of preventing UV-driven photodamage and related pathologies by topical PD-L1 antagonism.

On the basis of PD-L1 responsiveness in sun-damaged human skin and the findings that topical BMS-202 application can suppress solar UV-induced AP-1 activation, inflammatory gene expression, PD-L1 upregulation, and caspase-3 cleavage in SKH-1 mouse skin, pharmacological strategies using topical PD-L1 antagonism warrant further studies targeting human skin photodamage.

MATERIALS AND METHODS

Human specimens, immunohistochemistry, and RPPA

Human tumor samples and skin biopsies were obtained under protocols approved by the University of Arizona institutional review board (institutional review board number 1807818073), all samples

were deidentified, and written informed consent was documented. Samples were classified as normal SP skin ($n = 20$), low-risk cSCC ($n = 39$), or high-risk cSCC ($n = 30$) using clinical evaluation and verification from pathological analysis according to the Brigham and Women's Hospital staging system (Karia et al, 2014). IHC staining of human skins for PD-L1 was performed as described previously using the SP263 kit (Ventana Medical Systems) (Dickinson et al, 2021). Staining of tissue sections was measured using ImageProPlus (Media Cybernetics), a Leica DMR microscope, and a Sony 3CCD color video camera (Bermudez et al, 2015). For all tissues (epidermis or cSCC), analysis was confined to keratinocytic cells. For human PD-L1, IHC tissue sections were independently scored by a dermatopathologist to determine the percentage of epidermis or tumor tissue staining positive for PD-L1, with a cutoff $\geq 5\%$ per field qualifying positive staining. For each marker, the percentage positive cytoplasmic area ($\times 40$ field) was determined per tissue specimen (averaging 3 fields). IHC images shown are magnified according to the 100 μm bar contained in the respective panel as specified throughout the figure legends. Statistical significance of differences in PD-L1 expression ($> 5\%$ between SP, low-risk cSCC, and high-risk cSCC) was tested using Kruskal–Wallis nonparametric data analysis (GraphPad Prism 10.0 software).

A second set of human skin biopsies, confirmed by a dermatopathologist to be normal (SP, buttock, $n = 21$) or sun damaged (forearm skin, $n = 10$ each for mild and moderate; $n = 8$ for severe), used macrodissection to separate the dermis from the epidermis. PD-L1 was quantified in epidermal lysates using proteomic analysis through RPPA as previously described (Baldelli et al, 2021; Dickinson et al, 2021). Briefly, RPPA was constructed using a 2470

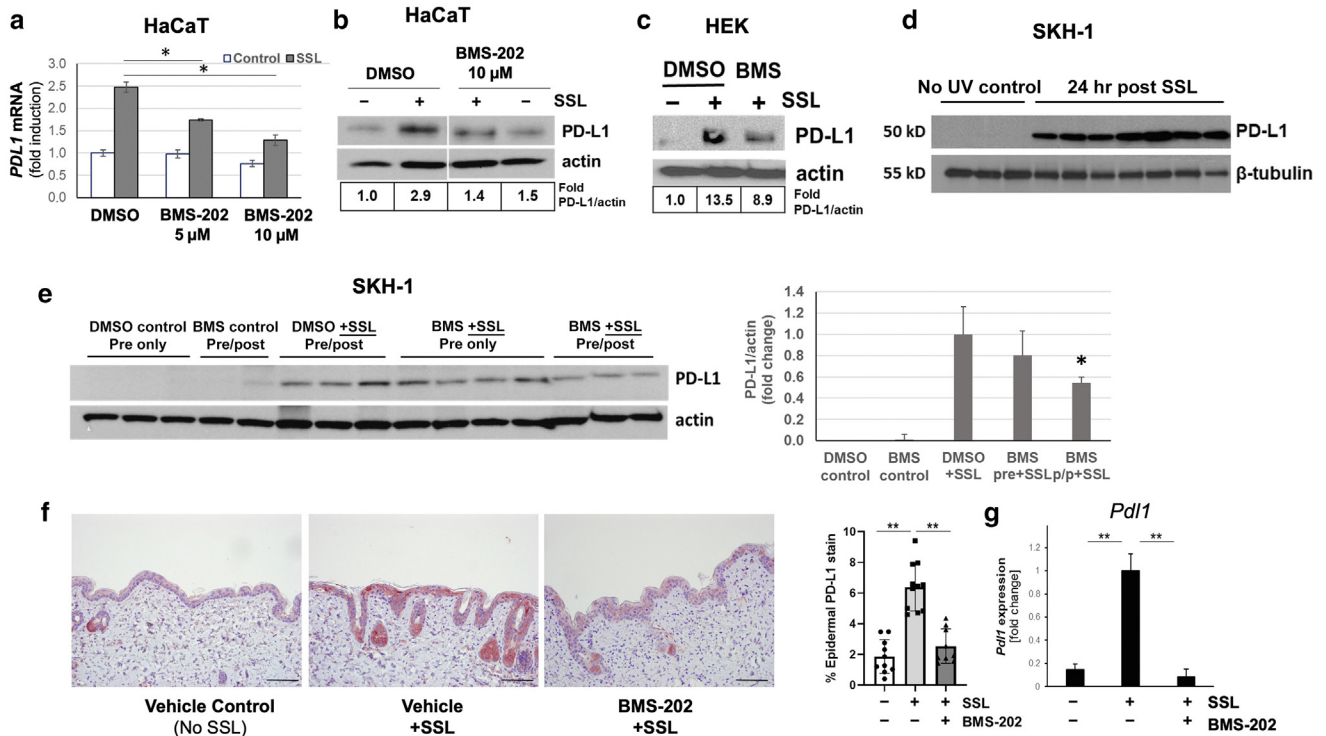


Figure 7. Effects of BMS-202 on SSL-induced PD-L1 upregulation in cultured human keratinocytes and SKH-1 mouse skin. (a) *Pdl1* mRNA expression (24 hr after SSL) is suppressed dose dependently by BMS-202 treatment in HaCaT keratinocytes. Data depict an experiment run in triplicate (and then repeated 2 more times; bars represent average ± SD). (b) Inhibition of SSL-induced PD-L1 protein upregulation examined by immunoblot analysis after treatment specified in a. (c) Inhibition of SSL-induced PD-L1 protein upregulation in primary epidermal keratinocytes examined as in b. (d) SSL-induced PD-L1 protein levels in treatment-naïve SKH-1 mouse epidermal lysates examined by immunoblot analysis. (e) Inhibition of SSL-induced PD-L1 protein upregulation in SKH-1 mouse epidermis due to topical BMS-202 (8 mM) as achieved before (only) or before and after treatment as determined by immunoblot analysis 24 hr after SSL (left). Data depict individual mouse samples on the left (n = 3), with bar graph analysis on the right (average ± SD; representative experiment of 3 independent repeats). (f) Immunohistochemistry of pre/post-treated SKH-1 skin as in e, stained for PD-L1 (left, bar = 100 μm). The bar graph (right) depicts the quantification of epidermal staining. (g) *Pdl1* mRNA expression (24 hr after SSL) in SKH-1 mouse skin topically treated with 8 mM BMS-202. In bar graphs, **P* ≤ 0.05 and ***P* ≤ .001. BMS, BMS-202; HEK, human epidermal keratinocyte; hr, hour; SSL, solar-simulated light.

Aushon Arrayer (Aushon BioSystems) equipped with 185 μm pins, and samples were immobilized onto nitrocellulose-coated glass slides (Grace Biolabs) in technical replicates (n = 3). PD-L1 levels were measured using a commercially available tyramide-based Catalyzed Signal Amplification System (Dako) coupled with a fluorescent streptavidin-conjugated IRDye680 dye. Antibody- and Sypro Ruby Protein Blot–stained arrays were scanned with a laser PowerScanner (Tecan) using the appropriate wavelength channel. Image analysis was performed using commercially available software (MicroVigene, version 5.1.0.0, VigeneTech). The software automatically performs spot finding and subtraction of local background and unspecific signals. Samples were then normalized to the amount of protein and averaged across replicates. Log₂-transformed expression levels of PD-L1 (clone E1L3N) in the epidermis were shown by waterfall plot and box-and-whisker plots for the 4 groups of SP skin and mild, moderate, and severe sun-damaged skin samples. The 2 groups of SP and all sun-damaged samples were compared using generalized estimating equations to account for potential correlation of expression levels in SP and sun-damaged samples from the same patient.

Mouse irradiation

All mice were housed and treated in accordance with The University of Arizona Animal Care and Use Committee standards under an approved protocol (number 08-153). UVB exposure was performed on AP-1 luciferase reporter mice on the SKH-1 genetic background

at a dose of 2.75 kJ/m² using FS40 bulbs (Q-Lab) as described before with the modification that mice were imaged 24 hours after UVB exposure using whole-body bioluminescence instead of 48 hours after UVB using ear punches (Dickinson et al, 2009). SSL irradiation of SKH-1 mice (Charles River Laboratories, strain code 477) at a dose of 90 kJ/m² UVA/6 kJ/m² UVB was performed using UVA-340 bulbs (Q-Lab) as described before (Dickinson et al, 2016). No differences between male and female mice were noted in UV-induced PD-L1 cutaneous responses as published before, and most experiments displayed were conducted in male mice (Dickinson et al, 2021).

AP-1 SKH-1 reporter mouse bioluminescence

Male transgenic SKH-1 mice heterozygous for the TPA-Response Element–driven luciferase transgene (AP-1 luciferase mice, n = 3) were treated topically on their backs with 200 μl of 8 mM BMS-202 or vehicle control (acetone). For all mice receiving BMS-202, the compound was applied twice before (24 hours and 1 hour) as well as immediately after UV exposure, a dosing regimen ensuring efficient target modulation, similar to topical nonsunscreen photoprotection approaches published earlier (Blohm-Mangone et al, 2018; Janda et al, 2016). Mice were injected intraperitoneally with luciferin (potassium salt) stock solution in PBS without magnesium or calcium at a dose ≤150 mg/kg of body weight 24 hours after UV exposure and imaged (Lago instrument, Spectral Instruments Imaging) with Aura software analysis.

AP-1 reporter luciferase assay in HaCaT keratinocytes

HaCaT cells stably transfected with the TPA-Response Element-driven luciferase plasmid (AP-1 luciferase cells) were seeded in 6-well plates, grown to 70% confluence, and serum starved overnight to reduce background signaling. Cells were pre-treated with BMS-202 or vehicle (DMSO) for 1 hour and then washed twice with PBS before exposure to 250 kJ/m² UVB as described previously (Dickinson et al, 2009; Janda et al, 2016). Cells were then washed once more with PBS before being placed into fresh starvation media with vehicle or BMS-202 until harvest 12 hours later. Cells were lysed in Promega's Cell Culture Lysis Buffer, and a total of 10 µg protein per sample replicate was assayed for luciferase activity according to the manufacturer's instructions for the Luciferase Assay System (Promega) using a TD 20/20 luminometer (Turner Designs). Experimental triplicates were averaged, and the means from each independent experiment were analyzed by Student's *t*-test for statistical significance. Results are representative of 3 independent experiments.

RT-qPCR gene expression analysis

Total RNA was isolated from SSL-treated mouse skin using the Qiagen RNeasy Mini Kit (Qiagen) according to the manufacturer's instructions. RNA integrity was checked by the RNA 6000 Nano chip kit using Agilent 2100 Bioanalyzer (Agilent Technologies). Mouse 20X primer/probes (*Il6* [Mm_00446190_m1], *Il0* [Mm_01288386_m1], *Il1b* [Mm_00434228_m1], *Tnf* [Mm_00443258_m1], *Tlr4* [Mm_00445273_m1], *Ptgs2* [Mm_00478374_m1], *Pdli* [Mm_00452054_m1], *Rps18* [housekeeping gene; Mm_02601777_g1]) were obtained from Thermo Fisher Scientific. A total of 500 ng of total RNA was used for cDNA synthesis using the following cycling conditions: 25 °C for 10 minutes, 48 °C for 30 minutes, and 95 °C for 5 minutes performed in MJ Thermocycler PTC-200 (MJ Research). Then, 10 ng of cDNA was used for amplification of target genes by quantitative PCR using the following conditions: 95 °C for 10 minutes followed by 95 °C for 15 seconds and 60 °C for 1 minute for a total of 40 cycles performed in the ABI7500 Real-Time PCR System (Applied Biosystems). PCR amplification of the human housekeeping gene *RPS18* was used to control the quality of the cDNA. Nontemplate controls were included on each PCR plate. Expression levels of target genes were normalized to the *RPS18* control ($\Delta Ct = Ct [\text{gene of interest}] - Ct [\text{housekeeping gene}]$). After amplification plots were generated, and the Ct values (cycle number at which fluorescence reaches threshold) were recorded and quantified using the comparative ($\Delta\Delta Ct$) Ct method as described in the ABI Prism 7500 sequence detection system user guide (Cabello et al, 2009; Davis et al, 2015; Jandova et al, 2020). Statistical significance was calculated employing the Student's 2-tailed *t*-test.

Mouse immunohistochemistry

Caspase-3. Briefly, deparaffinized mouse skin slides were subjected to antigen retrieval using a Decloaking chamber in Rodent Decloaker HIER solution (both from Biocare, 115 °C for 30 seconds, then 90 °C for 10 seconds) followed by blocking with first 3% hydrogen peroxide (10 minutes) and then 5% normal goat serum in PBS with Tween 20 (1 hour). Slides were then incubated in a 1:300 dilution of anticlaved caspase-3 antibody (number 9661, Cell Signal Technology) at 4 °C overnight. Detection utilized a Vectastain ABC immunoperoxidase kit (PD-6100) with a biotinylated anti-rabbit IgG secondary antibody (Vector Laboratories, BA-1000) and

NovaRED substrate according to the manufacturer's instructions. Negative control slides were exposed to secondary antibody only and displayed no detectable staining (data not shown). Slides were counterstained in dilute Hematoxylin Gill III for 2 seconds (Leica Biosystems). For quantification, the average count (caspase 3 positive per total epidermal cells) in 4 fields per slide ($\times 20$ field) was determined for each mouse skin specimen and calculated per group ($n = 3$).

PD-L1. IHC staining for PD-L1 in mouse skins was performed using the NBP1-43262 antibody (Novus) as described previously (Dickinson et al, 2021). Epidermal PD-L1 expression is shown as percentage staining determined by ImageJ (National Institutes of Health, open source) quantification using color deconvolution of the brown stain with a uniform threshold between all samples. Each skin sample ($n = 3$, $\times 20$ field) was used to measure at least 3 fields per specimen with exclusion of hair follicles, if present.

Mouse IHC data were analyzed using Kruskal–Wallis nonparametric data analysis (GraphPad Prism 10.0 software). IHC images shown are magnified according to the 100 µm bar contained in the respective panel as specified throughout the figure legends.

NanoString nCounter gene expression analysis

SKH-1 mouse skin (full thickness, 3 biological samples [ie, 3 mice per treatment group]) was treated either with vehicle (acetone) or 8 mM BMS-202 (all 3 times: 24 hours before, 1 hour before, and immediately after) and harvested 24 hours after acute SSL. First, total mRNA was prepared using the RNeasy Mini kit (Qiagen). Next, 100 ng was used for NanoString nCounter analysis (using the Mouse Inflammation V2 panel; probing 254 genes, NanoString Technologies) comparing gene expression between treatment groups (Geiss et al, 2008; Kulkarni, 2011). Total mRNA was hybridized with the Mouse Inflammation V2 code set at 65 °C overnight. Further purification and binding of the hybridized probes to the optical cartridge was performed on the nCounter Prep Station, and finally, the cartridge was scanned on the nCounter Digital Analyzer. Reporter Code Count (RCC) files were then imported into nSolver4.0 software (NanoString Technologies) and checked for data quality using default quality control settings; all samples passed data quality control. All samples were normalized using the geometric mean of the housekeeper genes. Expression ratios were calculated by dividing the mean values of all samples in one experimental group (UV+ BMS-202) by the mean values of all samples in the reference group (UV+ vehicle control). For data analysis, low count threshold value was 200. For heatmap depiction (Figures 3, 5, and 6), a z-score for a specific gene indicates the number of SDs away from the mean of expression in the reference samples. For pathway score analysis (Figure 4), each sample's gene expression profile was then condensed into a small set of pathway scores using nCounter Advanced Analysis software (version 2.0.115). Pathway scores were fit using the first principal component of each gene set's data, oriented such that each pathway score has positive weights for at least half its genes. A covariate plot displays selected pathway scores against the covariate chosen (ie, BMS-202 treatment). Numerical pathway score represents the average fold expression change for all genes associated with the specific pathway, with positive scores indicating enhancement and negative scores indicating attenuation; scores are displayed on the same scale through a Z-transformation.

Individual samples were run in triplicate format of biological replicates, and data analysis was performed using the nSolver analysis software (4.0). For *P*-value adjustment (Benjamini–Yekutieli

false discovery rate; P -value threshold = .05), nCounter Advanced Analysis software (version 2.0.115) was used. Nonparametric data analysis of murine experimentation was performed using the Mann–Whitney test. Differences between groups were considered significant at $*P < .05$.

Cell culture and SSL treatment

Human HaCaT immortalized keratinocytes were maintained in DMEM with 10% fetal bovine serum and $1 \times$ penicillin/streptomycin. Cells were authenticated using short tandem repeat (STR) genotype analysis and tested for mycoplasma regularly. Cells were seeded onto 60 cm dishes at a density of ~ 200 k/dish and grown for 3 days. Before treatment, cells were serum starved overnight to enhance UV responsiveness of signaling. Cells were $\sim 80\%$ confluent at the time of treatment. BMS-202 (10 μM) in DMSO was added to the media 1 hour before SSL (pretreatment).

For SSL treatment, UVA-340 bulbs (Q-Lab) were used as published (Dickinson et al, 2021). Before exposure, cells were washed with $1 \times$ PBS and then incubated in 4 ml PBS (with 0.01% magnesium chloride and 0.01% calcium chloride) during irradiation. Cells were exposed to 40 kJ/m^2 UVA/2.68 kJ/m^2 UVB and then rinsed once more with PBS before being placed back into DMEM with 1% fetal bovine serum + penicillin/streptomycin and vehicle or BMS-202 (after treatment) and incubated until harvest 24 hours later. Control cells underwent identical processing except that they were held in the biosafety cabinet without UV exposure.

Adult human epidermal keratinocytes were purchased from Thermo Fisher Scientific and maintained in EpiLife media on collagen-coated plates as per the vendor's instructions. Cells were treated with BMS-202 and SSL as described for HaCaT cells.

Immunoblot analysis (cell culture and mouse epidermis)

Cells were lysed in RIPA containing $1 \times$ HALT protease + phosphatase inhibitor cocktail (Thermo Fisher Scientific), and 100 mM phenylmethylsulfonyl fluoride and protein concentrations were assessed using BCA assay (Bio-Rad Laboratories). Mouse epidermal protein lysates for immunoblot analysis were derived from scraped frozen SKH-1 skins as described previously (Blohm-Mangone et al, 2018). A total of 20 μg of protein/lane was loaded onto 10% gels for electrophoresis/immunoblotting using established protocols. Human cell lysate blots were probed with Cell Signaling PD-L1 antibody (number 13684), and mouse epidermal lysate blots were probed with Invitrogen PD-L1 antibody (number PA5 – 20343). β -Actin (Cell Signaling Technology, number 4970) was used as a loading control. An anti-rabbit secondary antibody (Cell Signaling Technology, number 7074) was used for all blots using standard chemiluminescent protocols (Thermo Fisher Scientific Pico ECL, number 34577). Densitometric analysis of band intensity was performed using ImageJ (National Institutes of Health, open source).

ETHICS STATEMENT

All participants provided written, informed consent, and this protocol was approved by the institutional review board of the University of Arizona (protocol title: Skin Cancer Prevention Program Biorepository; protocol number 120000229). Animal studies were performed in accordance with The University of Arizona Animal Care and Use Committee standards under an approved protocol (number 08-153).

DATA AVAILABILITY STATEMENT

All gene array expression data generated in this study are disclosed and presented in the manuscript. NanoString nCounter–derived large datasets were deposited in the National Center for Biotechnology Information gene

expression omnibus repository database (public on December 19, 2023): <https://www.ncbi.nlm.nih.gov/geo/query/acc.cgi?acc=GSE250046>. According to Gene Expression Omnibus accession display, data were generated using the GPL20885 nCounter Mouse Inflammation panel V2 panel: <https://www.ncbi.nlm.nih.gov/geo/query/acc.cgi?acc=GPL20885>

ORCIDs

Sally E. Dickinson: <http://orcid.org/0000-0002-2049-543X>
 Prajakta Vaishampayan: <http://orcid.org/0009-0003-0356-7061>
 Jana Jandova: <http://orcid.org/0000-0002-9100-9574>
 Yuchen (Ella) Ai: <http://orcid.org/0009-0007-3484-6927>
 Viktoria Kirschnerova: <http://orcid.org/0000-0001-8810-1321>
 Tianshun Zhang: <http://orcid.org/0000-0001-7018-8393>
 Valerie Calvert: <http://orcid.org/0000-0002-5075-7728>
 Emanuel Petricoin III: <http://orcid.org/0000-0001-8787-5990>
 H-H. Sherry Chow: <http://orcid.org/0000-0002-9638-711X>
 Chengcheng Hu: <http://orcid.org/0000-0001-8525-0356>
 Denise Roe: <http://orcid.org/0000-0001-6989-6579>
 Ann Bode: <http://orcid.org/0000-0002-7432-082X>
 Clara Curiel-Lewandrowski: <http://orcid.org/0000-0001-8982-6252>
 Georg T. Wondrak: <http://orcid.org/0000-0003-4799-8608>

CONFLICT OF INTEREST

The authors state no conflict of interest.

ACKNOWLEDGMENTS

This work was supported by the National Institutes of Health/National Cancer Institute (P01 CA229112, R01 CA229418, P30 CA023074), The University of Arizona Cancer Center Skin Cancer Institute, and the Janice and Alan Levine Endowed Chair in Cancer Research. The authors thank Mary Krutzsch and Michael Yozwiak for their excellent technical support.

AUTHOR CONTRIBUTIONS

Conceptualization: SED, GTW, CC-L; Data Curation: SED, PV, JJ, CH, GTW; Formal Analysis: SED, JJ, CH, DR, GTW; Funding Acquisition: SED, TZ, AB, H-HSC, CC-L, GTW; Investigation: SED, PV, JJ, Y(E)A, VK, VC, EP, CC-L, GTW; Methodology: SED, GTW, CC-L; Project Administration: SED, CC-L, GTW; Resources: SED, EP, DR, CC-L, GTW; Software: CH, DR; Supervision: SED, EP, TZ, AB, H-HSC, CC-L, GTW; Validation: PV, VK, JJ, VC, SED, GTW; Visualization: SED, PV, JJ, CH, GTW; Writing – Original Draft Preparation: SED, GTW; Writing – Review and Editing: SED, EP, CH, GTW, CC-L

REFERENCES

- Ashizawa T, Iizuka A, Tanaka E, Kondou R, Miyata H, Maeda C, et al. Anti-tumor activity of the PD-1/PD-L1 binding inhibitor BMS-202 in the humanized MHC-double knockout NOG mouse. *Biomed Res* 2019;40:243–50.
- Baldelli E, Hodge KA, Bellezza G, Shah NJ, Gambaro G, Sidoni A, et al. PD-L1 quantification across tumor types using the reverse phase protein microarray: implications for precision medicine. *J Immunother Cancer* 2021;9:e002179.
- Bermudez Y, Stratton SP, Curiel-Lewandrowski C, Warneke J, Hu C, Bowden GT, et al. Activation of the PI3K/Akt/mTOR and MAPK signaling pathways in response to acute solar-simulated light exposure of human skin. *Cancer Prev Res (Phila)* 2015;8:720–8.
- Blohm-Mangone K, Burkett NB, Tahsin S, Myrdal PB, Aodah A, Ho B, et al. Pharmacological TLR4 antagonism using topical resatorvid blocks solar UV-induced skin tumorigenesis in SKH-1 mice. *Cancer Prev Res (Phila)* 2018;11:265–78.
- Blum V, Müller B, Hofer S, Pardo E, Zeidler K, Diebold J, et al. Nivolumab for recurrent cutaneous squamous cell carcinoma: three cases. *Eur J Dermatol* 2018;28:78–81.
- Cabello CM, Bair WB 3rd, Lamore SD, Ley S, Bause AS, Azimian S, et al. The cinnamon-derived Michael acceptor cinnamic aldehyde impairs melanoma cell proliferation, invasiveness, and tumor growth. *Free Radic Biol Med* 2009;46:220–31.
- Cadet J, Mouret S, Ravanat JL, Douki T. Photoinduced damage to cellular DNA: direct and photosensitized reactions. *Photochem Photobiol* 2012;88:1048–65.
- Cao Y, Zhang L, Kamimura Y, Ritprajak P, Hashiguchi M, Hirose S, et al. B7-H1 overexpression regulates epithelial-mesenchymal transition and accelerates carcinogenesis in skin. *Cancer Res* 2011a;71:1235–43.

- Cao Y, Zhang L, Ritprajak P, Tsushima F, Youngnak-Piboonratanakit P, Kamimura Y, et al. Immunoregulatory molecule B7-H1 (CD274) contributes to skin carcinogenesis. *Cancer Res* 2011b;71:4737–41.
- Chen W, Borchers AH, Dong Z, Powell MB, Bowden GT. UVB irradiation-induced activator protein-1 activation correlates with increased c-fos gene expression in a human keratinocyte cell line. *J Biol Chem* 1998;273:32176–81.
- Clydesdale GJ, Dandie GW, Muller HK. Ultraviolet light induced injury: immunological and inflammatory effects. *Immunol Cell Biol* 2001;79:547–68.
- Constantinidou A, Alifieris C, Trafalis DT. Targeting programmed cell death -1 (PD-1) and Ligand (PD-L1): a new era in cancer active immunotherapy. *Pharmacol Ther* 2019;194:84–106.
- Cooper SJ, Bowden GT. Ultraviolet B regulation of transcription factor families: roles of nuclear factor-kappa B (NF-kappaB) and activator protein-1 (AP-1) in UVB-induced skin carcinogenesis. *Curr Cancer Drug Targets* 2007;7:325–34.
- Dai MY, Shi YY, Wang AJ, Liu XL, Liu M, Cai HB. High-potency PD-1/PD-L1 degradation induced by Peptide-Protac in human cancer cells. *Cell Death Dis* 2022;13:924.
- Davis AL, Qiao S, Lesson JL, Rojo de la Vega M, Park SL, Seanez CM, et al. The quinone methide aurin is a heat shock response inducer that causes proteotoxic stress and Noxa-dependent apoptosis in malignant melanoma cells. *J Biol Chem* 2015;290:1623–38.
- Dickinson SE, Janda J, Criswell J, Blohm-Mangone K, Olson ER, Liu Z, et al. Inhibition of Akt enhances the chemopreventive effects of topical rapamycin in mouse skin. *Cancer Prev Res (Phila)* 2016;9:215–24.
- Dickinson SE, Khawam M, Kirschnerova V, Vaishampayan P, Centuori SM, Saboda K, et al. Increased PD-L1 expression in human skin acutely and chronically exposed to UV irradiation. *Photochem Photobiol* 2021;97:778–84.
- Dickinson SE, Melton TF, Olson ER, Zhang J, Saboda K, Bowden GT. Inhibition of activator protein-1 by sulforaphane involves interaction with cysteine in the cFos DNA-binding domain: implications for chemoprevention of UVB-induced skin cancer. *Cancer Res* 2009;69:7103–10.
- Dickinson SE, Olson ER, Zhang J, Cooper SJ, Melton T, Criswell PJ, et al. p38 MAP kinase plays a functional role in UVB-induced mouse skin carcinogenesis. *Mol Carcinog* 2011;50:469–78.
- Geiss GK, Bumgarner RE, Birditt B, Dahl T, Dowidar N, Dunaway DL, et al. Direct multiplexed measurement of gene expression with color-coded probe pairs. *Nat Biotechnol* 2008;26:317–25.
- Gou Q, Dong C, Xu H, Khan B, Jin J, Liu Q, et al. PD-L1 degradation pathway and immunotherapy for cancer. *Cell Death Dis* 2020;11:955.
- Green MR, Rodig S, Juszczynski P, Ouyang J, Sinha P, O'Donnell E, et al. Constitutive AP-1 activity and EBV infection induce PD-L1 in Hodgkin lymphomas and posttransplant lymphoproliferative disorders: implications for targeted therapy [published correction appears in *Clin Cancer Res* 2012;18:2117] *Clin Cancer Res* 2012;18:1611–8.
- Guy GP Jr, Machlin SR, Ekwueme DU, Yabroff KR. Prevalence and costs of skin cancer treatment in the U.S., 2002–2006 and 2007–2011. *Am J Prev Med* 2015;48:183–7.
- Guzik K, Zak KM, Grudnik P, Magiera K, Musielak B, Törner R, et al. Small-molecule inhibitors of the programmed cell Death-1/Programmed death-ligand 1 (PD-1/PD-L1) interaction via transiently induced protein states and dimerization of PD-L1. *J Med Chem* 2017;60:5857–67.
- Hanks BA. The "inside" story on tumor-expressed PD-L1. *Cancer Res* 2022;82:2069–71.
- Hu Z, Yu P, Du G, Wang W, Zhu H, Li N, et al. PCC0208025 (BMS202), a small molecule inhibitor of PD-L1, produces an antitumor effect in B16-F10 melanoma-bearing mice [published correction appears in *PLoS One* 2021;16:e0251020] *PLoS One* 2020;15:e0228339.
- Hudson K, Cross N, Jordan-Mahy N, Leyland R. The extrinsic and intrinsic roles of PD-L1 and its receptor PD-1: implications for immunotherapy treatment. *Front Immunol* 2020;11:568931.
- Imai Y, Ayithan N, Wu X, Yuan Y, Wang L, Hwang ST. Cutting edge: PD-1 regulates imiquimod-induced psoriasisform dermatitis through inhibition of IL-17A expression by innate $\gamma\delta$ -low T cells. *J Immunol* 2015;195:421–5.
- Janda J, Burkett NB, Blohm-Mangone K, Huang V, Curiel-Lewandrowski C, Alberts DS, et al. Resatorvid-based pharmacological antagonism of cutaneous TLR4 blocks UV-induced NF-kB and AP-1 signaling in keratinocytes and mouse skin. *Photochem Photobiol* 2016;92:816–25.
- Jandova J, Perer J, Hua A, Snell JA, Wondrak GT. Genetic target modulation employing CRISPR/Cas9 identifies glyoxalase 1 as a novel molecular determinant of invasion and metastasis in A375 human malignant melanoma cells in vitro and in vivo. *Cancers (Basel)* 2020;12:1369.
- Jandova J, Snell J, Hua A, Dickinson S, Fimbres J, Wondrak GT. Topical hypochlorous acid (HOCl) blocks inflammatory gene expression and tumor-igenic progression in UV-exposed SKH-1 high risk mouse skin. *Redox Biol* 2021;45:102042.
- Karia PS, Han J, Schmults CD. Cutaneous squamous cell carcinoma: estimated incidence of disease, nodal metastasis, and deaths from disease in the United States, 2012. *J Am Acad Dermatol* 2013;68:957–66.
- Karia PS, Jambusaria-Pahlajani A, Harrington DP, Murphy GF, Qureshi AA, Schmults CD. Evaluation of American Joint Committee on Cancer, International Union Against Cancer, and Brigham and Women's Hospital tumor staging for cutaneous squamous cell carcinoma. *J Clin Oncol* 2014;32:327–34.
- Kulkarni MM. Digital multiplexed gene expression analysis using the NanoString nCounter system. *Curr Protoc Mol Biol* 2011. Chapter 25:Unit25B.10.
- Lin C, Ballah T, Nottage M, Hay K, Chua B, Kenny L, et al. A prospective study investigating the efficacy and toxicity of definitive chemoradiation and Immunotherapy (CRIO) in locally and/or regionally advanced unresectable cutaneous squamous cell carcinoma. *Radiat Oncol* 2021;16:69.
- Madan V, Lear JT, Szeimies RM. Non-melanoma skin cancer. *Lancet* 2010;375:673–85.
- Malaspina TS, Gasparoto TH, Costa MR, de Melo EF Jr, Ikoma MR, Damante JH, et al. Enhanced programmed death 1 (PD-1) and PD-1 ligand (PD-L1) expression in patients with actinic cheilitis and oral squamous cell carcinoma. *Cancer Immunol Immunother* 2011;60:965–74.
- Mansouri B, Housewright CD. The treatment of actinic keratoses—the rule rather than the exception. *JAMA Dermatol* 2017;153:1200.
- Okiyama N, Katz SI. Programmed cell death 1 (PD-1) regulates the effector function of CD8 T cells via PD-L1 expressed on target keratinocytes. *J Autoimmun* 2014;53:1–9.
- Padmanabhan R, Kheraldine H, Gupta I, Meskin N, Hamad A, Vranic S, et al. Quantification of the growth suppression of HER2+ breast cancer colonies under the effect of trastuzumab and PD-1/PD-L1 inhibitor. *Front Oncol* 2022;12:977664.
- Rhodes LE, Gledhill K, Masoodi M, Haylett AK, Brownrigg M, Thody AJ, et al. The sunburn response in human skin is characterized by sequential eicosanoid profiles that may mediate its early and late phases. *FASEB J* 2009;23:3947–56.
- Ritprajak P, Azuma M. Intrinsic and extrinsic control of expression of the immunoregulatory molecule PD-L1 in epithelial cells and squamous cell carcinoma. *Oral Oncol* 2015;51:221–8.
- Schaper K, Köther B, Hesse K, Satzger I, Gutzmer R. The pattern and clinicopathological correlates of programmed death-ligand 1 expression in cutaneous squamous cell carcinoma. *Br J Dermatol* 2017;176:1354–6.
- Shaulian E, Karin M. AP-1 in cell proliferation and survival. *Oncogene* 2001;20:2390–400.
- Slater NA, Googe PB. PD-L1 expression in cutaneous squamous cell carcinoma correlates with risk of metastasis. *J Cutan Pathol* 2016;43:663–70.
- Snell JA, Vaishampayan P, Dickinson SE, Jandova J, Wondrak GT. The drinking water and swimming pool disinfectant Trichloroisocyanuric acid causes chlorination stress enhancing solar UV-induced inflammatory gene expression in AP-1 transgenic SKH-1 luciferase reporter mouse skin. *Photochem Photobiol* 2023;99:835–43.
- Stravodimou A, Tzelepi V, Balasis S, Georgiou S, Papadaki H, Mouzaki A, et al. PD-L1 expression, T-lymphocyte subpopulations and Langerhans cells in cutaneous squamous cell carcinoma and precursor lesions. *Anti-cancer Res* 2021;41:3439–48.
- Sun C, Yin M, Cheng Y, Kuang Z, Liu X, Wang G, et al. Novel small-molecule PD-L1 inhibitor induces PD-L1 internalization and optimizes the immune microenvironment. *J Med Chem* 2023;66:2064–83.

Umar A. Cancer immunoprevention: a new approach to intercept cancer early. *Cancer Prev Res (Phila)* 2014;7:1067–71.

Vaishampayan P, Curiel-Lewandrowski C, Dickinson SE. Review: PD-L1 as an emerging target in the treatment and prevention of keratinocytic skin cancer. *Mol Carcinog* 2023;62:52–61.

Wondrak GT, Jacobson MK, Jacobson EL. Endogenous UVA-photosensitizers: mediators of skin photodamage and novel targets for skin photoprotection. *Photochem Photobiol Sci* 2006;5:215–37.

Zak KM, Grudnik P, Magiera K, Dömling A, Dubin G, Holak TA. Structural biology of the immune checkpoint receptor PD-1 and its ligands PD-L1/PD-L2. *Structure* 2017;25:1163–74.

Zerdes I, Matikas A, Bergh J, Rassidakis GZ, Foukakis T. Genetic, transcriptional and post-translational regulation of the programmed death protein ligand 1 in cancer: biology and clinical correlations. *Oncogene* 2018;37:4639–61.

Zhang R, Zhu Z, Lv H, Li F, Sun S, Li J, et al. Immune checkpoint blockade mediated by a small-molecule nanoinhibitor targeting the PD-1/PD-L1 pathway synergizes with photodynamic therapy to elicit antitumor immunity and antimetastatic effects on breast cancer. *Small* 2019;15:e1903881.

Zhong SP, Ma WY, Quealy JA, Zhang Y, Dong Z. Organ-specific distribution of AP-1 in AP-1 luciferase transgenic mice during the maturation process. *Am J Physiol Regul Integr Comp Physiol* 2001;280:R376–81.



This work is licensed under a Creative Commons Attribution-NonCommercial-NoDerivatives 4.0 International License. To view a copy of this license, visit <http://creativecommons.org/licenses/by-nc-nd/4.0/>